

Regaining Sense of Touch:  
Artificial, Pressure-sensitive Skin for  
Hand Prosthetics

*Within*

BIOMEDICAL ENGINEERING

*Written by*

AXEL EKMAN

*Supervised by*

CHRISTIAN ANTFOLK

*And*

MARTIN BENGTSSON



**LUND**  
UNIVERSITY

DEPARTMENT OF  
BIOMEDICAL ENGINEERING

## Abstract

A large portion of upper-limb prosthesis users are known to defer the use of electronic prostheses due to their high cost, considerable weight and lack of durability. Within this thesis, an approach to simple, low-cost pressure feedback systems is made. Using commercially available pressure sensors and rudimentary materials such as PDMS and polycarbonate plastic, a working prototype for pressure-sensitive skin was constructed and subsequently tested for several membrane thicknesses corresponding to the thicknesses of an artificial skin. While minor issues remain regarding stability and leakage, the system shows great potential for simple and sensitive pressure sensing units with fast response times. Aside from mechanosensory units, the possibility of custom-made proprioceptors for prosthetic skin was also explored in the form of gold or copper strain gauges. All communication with the sensors was performed using an Arduino Nano unit programmed with a custom script included within this report and the data was collected and displayed using a custom LabView program.

## Preface

The documented work within this report was performed between March of 2015 and November of the same year, within the confines of the Department of Biomedical Engineering at Lund University's Faculty of Engineering.

The aim of this thesis project was to further the research within artificial skin for prosthetic hands, all the while focusing on keeping to a moderate budget with inexpensive materials and uncomplicated methods. Hopefully, the results of this research will serve as a basis for more, in-depth, research culminating in pressure-sensitive, moderately priced artificial skin able to relay a sensation of touch back to the user.

I thank Christian Antfolk, Martin Bengtsson and Lars Wallman for all their help and guidance. Special thanks to Axel Tojo for his help during circuit board manufacturing and to Cassandra Adams for her grammatical help and general support during the project work.

# Contents

<b>Abstract</b>	<b>1</b>
<b>Preface</b>	<b>2</b>
<b>Introduction</b>	<b>4</b>
<b>Goals and Restrictions</b>	<b>6</b>
<b>Theory</b>	<b>8</b>
Phantom Mapping . . . . .	8
Mechanoreception . . . . .	9
Proprioception . . . . .	10
<b>Methods and Resources</b>	<b>13</b>
Mechanoreception . . . . .	14
Proprioception . . . . .	18
<b>Implementation and Results</b>	<b>22</b>
Mechanoreception . . . . .	22
Iterative Implementation . . . . .	22
Data Collection . . . . .	26
Results . . . . .	29
Proprioception . . . . .	34
Results . . . . .	34
<b>Discussion</b>	<b>38</b>
Looking back and ahead . . . . .	40
<b>Concluding Remarks</b>	<b>45</b>
<b>References</b>	<b>46</b>
<b>Appendix A: Lab Protocol</b>	<b>48</b>
UV-mask . . . . .	48
Pattern Development . . . . .	48
Surface Protection . . . . .	49
PDMS Application . . . . .	49
<b>Appendix B: Arduino Code</b>	<b>50</b>

## Introduction

For a long time, the field of prosthetics was limited to stiff contraptions or peg-like substitutions. As our understanding of technology and medicine grew, however, a surge of innovation pushed the field to entirely new frontiers. Arguably the biggest leap within prosthetics came in the 20th century, when the field of prosthetics started to integrate with emerging microelectronics.

Presently, microelectronic integration has yielded many new possibilities for people with ablations of the limbs. A good example of this integration is the use of hand prosthetics controlled through subdermal neuronal potentiation, which allows users to control their prosthesis similarly to how they would control a natural limb.<sup>(1)</sup> After the emergence of such technology, the focus within the development of modern-day prosthetics quickly turned toward mimicking other aspects of the natural limb, such as sensory perception.

Still, in 2004, 70% of upper-limb prosthesis users in the United States preferred the use of hook contraptions over their electronic, hand-like counterparts. Most people in the corresponding minority reported that the reasons for using hand prosthetics instead of hooks were mostly aesthetic. This can be attributed to the fact that hand prosthetics, in general, offer less functionality than a hook and a much more steep learning curve. In addition to this, they are generally heavier and more expensive.<sup>(2)</sup> This loss of functionality can be derived from the lack of sensory feedback to both the prosthesis and its user, severely limiting any natural motion of the hand<sup>(3)</sup>.

Within this report, the sensing elements of a rudimentary prosthetic skin are proposed, where atmospheric pressure sensors are utilized in order to pick up tactile stimulation. These signals would then, theoretically, be transduced to the user's central nervous system, effectively regenerating a sense of touch. The

means of transduction can vary; electrical stimulation, pressure stimulation and vibration have previously been proposed by researchers as viable alternatives(4).

The outline of this report is as follows: first, goals and restrictions of the project are reviewed. Then, necessary theory behind proprioception and mechanoreception as well as phantom mapping are presented. Next, the sensors and other materials used are documented and their use is explained. After that, the experimental findings from each iteration of development are presented and briefly discussed. Lastly, the project is discussed as a whole together with future prospects of the proposed haptic system.

## Goals and Restrictions

The main goal within this project was to examine the sensing elements and the membrane material for an artificial skin for hand prosthetics able to offer pressure feedback.

It is important to note that there were no aspirations of creating novel materials in order to fulfil the functionality of the artificial skin. Instead, several materials were placed under scrutiny as candidates for component and circuit board use. For example, even though designing a custom pressure sensor might add to the project and the artificial skin itself, selecting between pressure sensors that were already on the market saved both time and resources. The skin's substrates for each phalange of a prosthetic finger were required to be both flexible and stiff in order to ensure proper bending of positional sensors without compromising the input of the pressure sensors. As such, rudimentary materials such as PDMS and polyimide were considered over novel materials found in research papers.

In order for the artificial skin to be compatible with hand prosthetics, a goal was set to incorporate sensors for basic object recognition as well as the above mentioned pressure sensing elements. These sensors —proprioceptors— were to be realized through the design and laboratory construction of flexible, high-angle metal foil strain gauges able to measure the flexion and extension of each finger.

In a study by Biddiss, Beaton and Chau from 2007, upper-limb prosthesis users were asked about their desired improvements to current prosthesis technology. The results of their research show that a lower prosthesis cost ranked within the top five design priorities for adult wearers of all device types. For electric devices in particular, the durability of prosthesis gloves and a lack of sensory feedback were deemed important areas of development.<sup>(5)</sup> Thus, two additional emphases within this project were placed onto achieving a low production cost of the finished product and

ensuring its durability. The notion of creating novel materials, mentioned above, was rejected mainly due to this restriction; the finished skin would ideally be durable and produced using low-cost materials and components, making it a viable option for the majority of upper-limb amputees.

A major restriction within this project was the implementation of the skin; only the development and testing of the skin components was included within its boundaries. The implementation and wiring of such a skin is thus left for another, future, venture.



## Theory

The human skin is complex in nature, utilizing a multitude of specialized sensors in order to feed relevant information back to the nervous system. In efforts to incorporate such a system with hand prosthetics, both mechanoreceptors and proprioceptors are paramount sensing components. Essentially, mechanoreceptors provide information regarding pressure applied to the tissue, whereas proprioceptors relay information regarding a sense of kinesthesia. That is, keeping track of the positions and movement of limbs and extremities in physical space.

### Phantom Mapping

The experiments herein are based off of the knowledge that most amputees who have suffered an ablation of the arm possess a so-called *phantom map* at the point of amputation. This phantom map connects areas of the skin with corresponding areas of the phantom limb, creating an essential informational bridge between stump and prosthesis. By exploiting this connection, sensory information can be relayed from the prosthesis to the amputee, essentially regenerating a sensation of touch.<sup>(6)</sup> For a simplified view of a phantom map applied to hand prosthetics, see Figure 1.

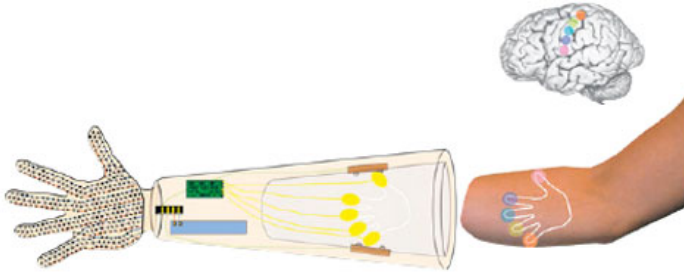


**Figure 1** – Simplified view of a phantom map being utilized for hand prosthetics; the stimulus for a specific digit on the prosthesis is relayed to the area of the stump which corresponds to the same phantom digit. Source: (6).

In 2012, C. Antfolk *et al.* showed that the results of sensory feedback mechanisms heavily depend on the completeness of the user's phantom map, and is independent of the feedback modality. That is, a less complete phantom map corresponds with poorer sensory discrimination and changing the means of transduction does not alter the phantom map.(7)

## Mechanoreception

When emulating the human skin using electronic pressure-sensing elements, the broad variety of sensors displayed in the natural skin is not easily accessible. Thus, regular pressure sensors would be required for implementation into the proposed artificial skin, seeing as they are the closest available electronic counterpart. In effect, each pressure sensor would transduce the same kind of information: pressure applied to the skin. Even though this only mirrors the most basic properties of the human mechanoreceptors, pressure sensors are still able to relay both a quantitative as well as a qualitative sense of pressure. Positioning pressure sensors on each phalange of a prosthetic hand, either integrated with or placed underneath the artificial skin, thus constitutes a basic model of a mechanoreceptive skin for hand prostheses.

The pressure sensors that were selected for this project are atmospheric pressure sensors based on MEMS-technology (MicroElec-

troMechanical Systems), where CMOS (Complementary Metal-Oxide Semiconductor) circuitry is hermetically sealed within a hard casing. The pressure inside and outside of the seal are compared; a piezoresistive element is deflected by pressure changes, which then relays information back to the integrated component interface. It is of importance to note that atmospheric pressure sensors are not normally intended for the type of use displayed within this project; the use of these sensors for prosthetic skin development was purely investigative in nature.

## Proprioception

The proprioceptive sensors, responsible for keeping track of each finger's position and movements, would be implemented in order to ensure appropriate grip functionality. Analogous proprioceptive components in the human body are, for example, muscle spindles and Golgi organs. Proprioception in an electrical context can be realized through several means of sensing, e.g. resistive gauging, fiber optics, pneumatics, or through utilization of the Hall effect. While each of these means have their respective advantages and disadvantages, the most commonly used sensor is a resistive gauge. These sensors are used with such prevalence due to their cheap, lightweight construction.<sup>(8)</sup> Resistive strain gauges can essentially be described as a winding metal path suitable for bending (see Figure 2).

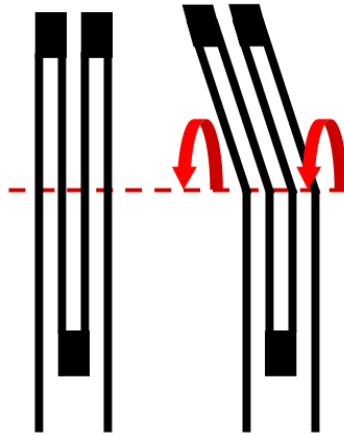


**Figure 2** – Schematic image of a resistive strain gauge. The right side of the image shows the intended bending of the example strain gauge on the left side.

Within this project, the proprioceptors were primarily realized through resistive gauges processed from gold-coated polyimide sheets. Another design of strain gauges was processed from copper-coated polyimide sheets through a copper etching process. The resistance of such strain gauges is dependent on the physical change in cross-sectional area. Assuming that the design is adequate, the output resistance of such a device can be modeled as such:

$$R = \rho \cdot \frac{l}{A} \quad (1)$$

Where  $\rho$  denotes electric resistivity,  $l$  corresponds to the length of the metal in the circuit and  $A$  to the cross-sectional area of the metal. As the cross-sectional area changes, voltage changes corresponding to the ensuing resistance change can be measured. Ideally, the voltage output would be measured across a Wheatstone bridge in order to remove any fluctuations due to temperature change.

When designing the above-mentioned sensors, the total resis-

tance was set at  $R_{tot} = 120 \Omega$  and the dimensions of the metal channel calculated using (1) while confining the height of the channel to the thickness of the metal layer. Naturally, self-designed strain gauges require characterization in order to be used properly, which can be achieved by measuring the angle of applied strain and comparing it to the change in resistance. In other words, plotting  $\frac{\Delta R}{R}$  versus the angle of strain,  $\theta$ . This also makes the result unitless and thus easier to compare to the characteristics of strain gauges with different  $R_{tot}$  values.

Even though strain gauges have previously been used within several industries (e.g. construction, where beams equipped with such sensors can relay information regarding their degree of bending back to a processing unit), the above-mentioned gauges differ from most other applications in one, important, aspect: industrial strain gauges are mainly used for extremely small angular changes, whereas the strain gauges needed for the artificial skin require bending on par with that of a human finger.

## Methods and Resources

The equipment and tools used for production and testing are listed below. Their uses are, if relevant, described within each respective sensor's subsection:

### *Pressure Sensors (Mechanoreception):*

- Computer
- DipTrace & LabView softwares
- Milling machine
- Empty copper circuit boards
- 3D-Printer (Ultimaker 2) & software (Cura)
- Elastosil for sealing
- Solder station & solder paste
- Light microscope
- Solder oven with reflow controller
- Arduino nano unit
- Breadboard & wiring
- DC voltage generator
- Connector headers
- 100nF capacitor
- 3.3V to 5V logic converter
- Multimeter
- XYZ-table
- Mountable force gauge (Mark-10 series 4)
- Sheets of Wacker Silicones Elastosil R401 Series (thicknesses 600 $\mu\text{m}$  & 1000 $\mu\text{m}$ ) & Sylgard170 mixed 1:1 (A:B) (thickness around 600 $\mu\text{m}$ )

### *Strain Gauges (Proprioception):*

- Computer

- AutoCAD software
- Factory-made polyimide film
- Au evaporator
- Mask writer
- UV-lithography station
- Laboratory chemicals as described in Appendix A
- Multimeter

## Mechanoreception

Initially, five types of pressure sensors were selected for use. These five sensors were mounted on a custom-made circuit board for testing purposes. However, due to time constraints, only the two most promising of the five sensors were picked for continued use. These were selected from their technical specifications, a few of which can be seen in table 1.

Property	Sensor A	Sensor B
Component Name	LPS25HB	BMP280
Manufacturer	ST Microelectronics	Bosch Sensortech
Interface	SPI & I <sup>2</sup> C	SPI & I <sup>2</sup> C
Absolute Pres- sure Range (hPa)	260 to 1260	300 to 1100
Dimensions L x W x H (mm)	2.5 x 2.5 x 0.76	2.0 x 2.5 x 0.95

**Table 1** – Selected technical specifications of the two pressure sensors used.

For each of the two remaining sensors, a custom circuit board was designed using the DipTrace software and subsequently milled using the department’s milling machine. The pressure sensors were surface mounted to their respective circuit boards by hand using solder paste and a light microscope. The solder paste was then activated using an oven connected to a reflow controller.

In order to prepare the sensors for use, two main methods were employed: one method aimed at creating a physical foundation around the sensor, allowing any applied pressure to be distributed evenly across the surface, and another method with no such foundation. Here, the pressure sensor was simply left as-is on the circuit board.

Utilizing the first method, square, plastic frames with inner dimensions of 16x16mm and a height of 5mm were 3D-printed and attached to some of the circuit boards using Elastosil as a sealant. After the Elastosil had settled, the excess elastomer seam was cut out using a scalpel and subsequently discarded, leaving a square space slightly smaller than 16x16mm around each pressure sensor. The frames were then filled with a two-part Sylgard170 elastomer mixed at a ratio of 1:1 (A:B) until the sensor was fully surrounded, but not covered. In order to see if the elastomer would have an effect on the sensor itself, one of each types of sensor was also fully covered with the Sylgard170. The applied volumes were initially calculated as the product of the surface area and the desired height of the membrane, but were later adjusted due to the elastomer clinging to the plastic framework. For a schematic overview of this setup, see Figure 3. For the remaining circuit boards, no frame was mounted and no elastomer cast, as mentioned above. Finally, both sets of circuit boards had connector pins soldered onto each end in order to enable communication.



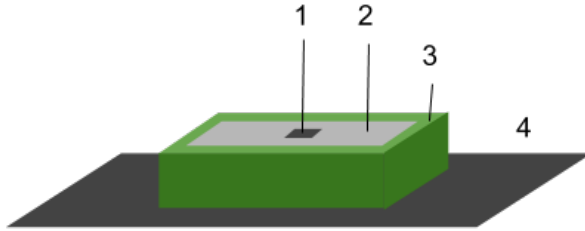


**Figure 3** – The first iteration of the experimental setup. Legend: 1) pressure sensor, 2) Sylgard170 filling, 3) 3D-printed plastic framework, 4) substrate (circuit board).

During the initial testing phase, communication with the devices was ensured through attachment to a breadboard. The breadboard was, in turn, connected to a ground, a DC voltage generator and an Arduino Nano unit. Additionally, the sensor was connected to a 100nF capacitor as per datasheet specification. The voltages relayed between the sensor and the Arduino were initially different and thus complicated communication (sensor pulled 3.3V and Arduino 5V). In order to remedy this, a 3.3V to 5V logic converter was connected between them. The Arduino was connected to a computer and subsequently programmed for an SPI interface matching each type of sensor. For a schematic view of the testing setup, please see Figure 4.

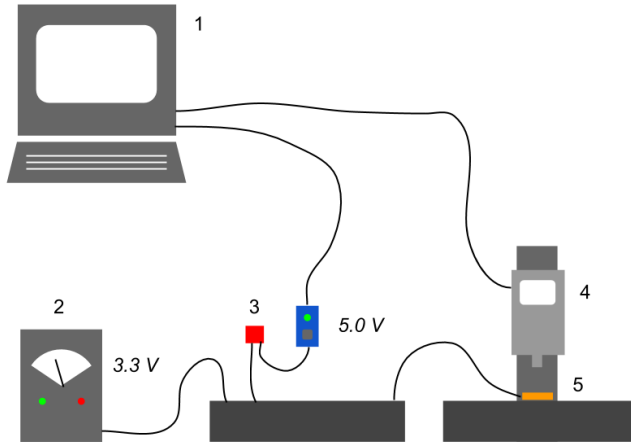


**Figure 4** – The setup rig used for testing. Legend: 1) desktop computer, 2) 3.3V voltage generator, 3) Arduino Nano unit and 3.3V to 5.0V logical converter, 4) force gauge mounted on the XYZ-table’s Z-axis, 5) pressure sensor mounted in the XYZ-table’s XY-plane.

During data collection, a communications cable was constructed which allowed for much greater freedom of movement for the circuit boards. Then, each pressure sensor was tested using an XYZ table (three mechanical axes maneuverable with high precision through a computer running a custom LabView software), where the circuit board carrying the surface mounted pressure sensor was fastened to the X and Y plane and stimulated using a Mark-10 force gauge attached to the Z axis. Both the pressure and force data were sent to a laboratory desktop computer (pressure data went through the Arduino unit) and were logged using a custom LabView program.

In order to test the combination of pressure sensors and elastomer membranes, roughly  $600\mu\text{m}$  thick sheets of Sylgard170 were created by depositing 1ml of the substance into a petri dish and let to flow freely at  $60^\circ\text{C}$ . These, along with factory-made PDMS (Wacker Silicones Elastosil R401 Series) sheets of  $600\mu\text{m}$  and 1mm, were then placed on top of the sensors right be-

fore testing. Throughout this thesis, the Wacker Silicones Elastosil R401 Series sheets are referred to simply as PDMS sheets, while Sylgard170 sheets are specified as such. For reference, the Young's modulus of the PDMS used was  $E=1.84\text{MPa}$ (9).

## Proprioception

The first iterations of metal foil strain sensors were designed in arrays using AutoCAD and made to fit on a ten by ten centimeter square. The pattern was then created as a glass mask for UV-lithography and through several steps of fabrication, gold-coated polyimide films were shaped into strain gauges. The details of the laboratory work can be seen in Appendix A: Lab Protocol. The pattern used for mask creation can be seen in Figure 5.

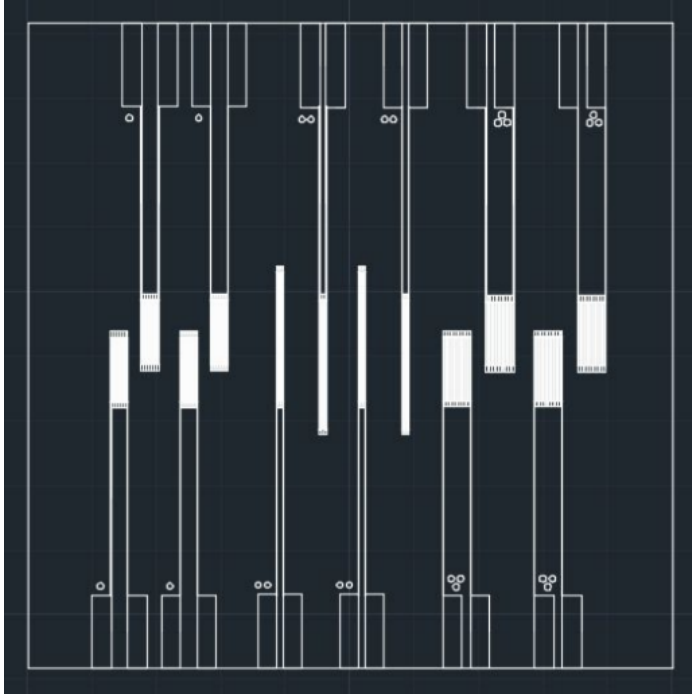


**Figure 5** – AutoCAD blueprint used for creating a UV lithography mask in order to create metal foil strain gauge sensors from gold-coated polyimide substrates. Each of the three designs is denoted as a collection of dots, ranging from one to three.

The finished and protected polyimide films containing the strain gauges were then contacted using two alternative methods: direct connection between external wiring and contact pad through the use of silver epoxy glue, and indirect connection between wiring and gauges using a copper array attached through conductive tape as an intermediate.

A second approach to strain gauge design was realized through the use of copper-coated polyimide sheets (Pyrallux sheets from Dupont). These were backed onto A4-paper and subsequently inserted into a solid ink printer (Xerox phaser 8560), where the desired circuit design was printed in pigmented wax directly onto the copper. The copper sheet was then etched in a standard

copper etching process for close to an hour, leaving only the ink-covered copper areas intact. The design of the copper sheets differed from that of the other gauges due to the fact that the copper method had not previously been performed at the department. Seeing as it was a new process, it was also decided that the smallest attainable resolution of the method should be investigated, hence the design which can be seen in Figure 6.

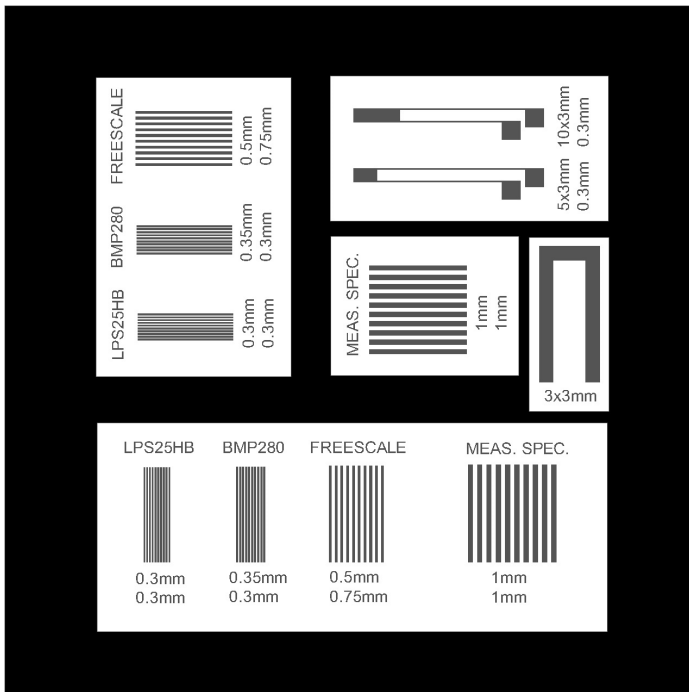


**Figure 6** – AutoCAD blueprint used for creating an ink jet printed mask in order to create metal foil strain gauge sensors from copper-coated polyimide substrates. The numbers beneath each design denote its relevant dimensions in the plane: the top numbers represent the line width of the sensing structures while the bottom numbers display the width between each line or the width of the connecting lines.

During testing, the strain gauge sheets were placed on a flat surface and the wires corresponding to each individual sensor's pads were attached to a multimeter. The resistance change was

noted as the middle of the sheet (the area containing the sensors) was carefully curved and, finally, bent. The multimeter was then connected to the next sensor's pads, and the procedure repeated. The exact angle of bending was not measured. All versions of strain gauges were tested in this manner.

## Implementation and Results

The process of getting reliable results out of the atmospheric pressure sensors became quite iterative, constantly improving upon methods and changing the setup. The results of each of these methods are presented below, and are briefly analyzed in order to justify the subsequent iterations. Similar iterative elements can be found in the process of strain gauge manufacturing, but their production was not as highly prioritized and thus did not continue as far the pressure-sensing systems.

### Mechanoreception

#### Iterative Implementation

The pressure sensors with a Sylgard170 base did not offer any relevant data, as the elastomer seems to have seeped into the sensing cavities and made them highly dependent on small temperature fluctuations instead of any pressure changes. The sensors would heat up quickly during applied pressure and showed very slow relaxation speeds. This seems to have been the case for all iterations where Sylgard170 was used in its liquid form around the sensor. Thus, it was decided to focus on the other circuit boards instead.

Where no elastomer base had been applied, the PDMS and Sylgard170 sheets were placed directly on top of the sensor before the force gauge was lowered in steps and data was collected. In order to determine how big of an effect the elastomer piece's area would have on the pressure output, small squares were cut from the 600 $\mu\text{m}$  and 1000 $\mu\text{m}$  PDMS sheets and subsequently placed on top of the sensor. The smallest square was modeled after the active sensing area on top of the LPS25HB unit and the second smallest square was made to fit the top surface area of the LPS25HB sensor. There was no major difference in pressure output, other than an abrupt increase in force at the point of compression where the force gauge hit the sensor casing through the PDMS, which happened more easily with smaller squares.

Unfortunately, there was a major problem with the system at this point: at constant forces, the pressure output would slowly rise. This could be due to the PDMS slowly creeping into the sensing cavities of the sensor that contain the pressure-sensitive membrane. As it crept further in, air would slowly be displaced, thus raising the pressure inside the chamber. To remedy this flaw, a new membrane was designed; the new membrane was raised from the sensor using spacers and gaskets, so as to avoid physical contact with the sensor.

The spacers were hand-crafted from 1.5mm thick sheets of polycarbonate or aluminum, cut to dimensions of 1.5x1.5cm and subsequently drilled, once, using a 3.7mm drill bit (for a snug fit around the LPS25HB sensor) and smoothed out using a 5mm drill bit rotated manually. Lastly, any sharp or uneven edges were filed down in an attempt to prevent air leakage and damage done to other components. For a schematic view, see Figure 8.

The first gasket iteration involved attaching a sheet of 600 $\mu$ m thick PDMS with a center hole the size of the LPS25HB sensor to the circuit board using elastosil. Attempts using this setup managed to prevent some of the problematic behaviors of the previous setup: mainly, leakage through the copper traces in the circuit board. Unfortunately, the system did not perform well and had issues with force stability. At this point, the aluminum spacers were discarded, since they were very uneven and warped from manufacture, which made them arduous to seal properly. Additionally, they did not show any preferential properties compared to the plastic spacers.

For the next iteration of the experimental setup, the gasket was re-sealed with elastosil and grease was applied in between the gasket and spacer, and in between the spacer and membrane. This removed the issue of leakage. However, grease unfortunately seeped into the sensor, rendering it useless.



Lastly, a final approach was made: another circuit board, identical to the previous one in its design, was utilized using only grease as a sealing agent. This meant that no elastomer gasket was sealed between the circuit board and the spacer. Using this setup, the total volume around the sensor was significantly decreased and better controlled (the elastomer could expand at high pressure changes, making the sensor less effective at measuring the pressure change). Additionally, only minor gas leakages were found, and the ones that persisted could almost entirely be remedied through the application of more grease. A visual representation of this system can be seen in Figure 7 and of the enclosed air volume in Figure 8.

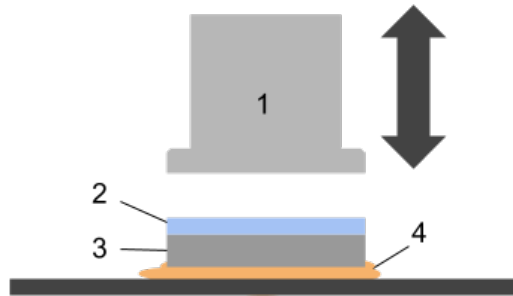


**Figure 7** – The final iteration of the experimental setup. Legend: 1) moveable force gauge, 2) PDMS membrane, 3) plastic spacer, 4) grease.

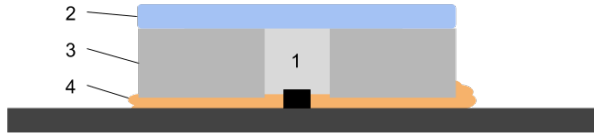


**Figure 8** – Schematic of the sensing cavity where air is displaced according to the PDMS membrane in order to create a measurable pressure change. Legend: 1) enclosed air sensing cavity with pressure sensor, 2) PDMS membrane, 3) plastic spacer, 4) grease.

Once the system was stable, data collection protocols were written in order to ensure consistency. The data was subsequently collected using the force gauge and XYZ-table setup described above. The two first protocols were designed to probe for the system's characterization curve (applying force in a quick step, then releasing back to zero force) and hysteresis effects (applying force in a quick step, then releasing down to half of the depression depth). The results from these experiments were found to be promising in regard to both response time and reproducibility. Therefore, two additional protocols were constructed: the first of the two (protocol three) was similar to the first protocol, but spanned across a larger interval of depression depth; the second of the two (protocol four) was similar to the second protocol, but repeated the hysteresis measurement cycle three times. It was constructed thusly in order to, in part, collect more data and, in part, to study the differences between short and significantly longer sessions of data collection.

For each of protocols three and four, measurements were made using each of these four membrane thicknesses:

- the membrane itself, a 600 $\mu\text{m}$  PDMS sheet attached with grease
- the 600 $\mu\text{m}$  membrane and another, identical albeit ungreased, 600 $\mu\text{m}$  PDMS sheet

- the 600 $\mu\text{m}$  membrane and a 1000 $\mu\text{m}$  ungreased PDMS sheet
- a 1000 $\mu\text{m}$  PDMS base membrane, attached with grease

Thus, the total membrane thicknesses used were 600 $\mu\text{m}$ , 1200 $\mu\text{m}$ , 1600 $\mu\text{m}$  and 1000 $\mu\text{m}$ . The 1000 $\mu\text{m}$  film is mentioned last since it has a thicker bottom membrane film than the other three. The Sylgard170 was excluded from these tests, as it was deemed to add unnecessary complexity to the measurements. This was decided due to the material's different Young's modulus, which was not given by the manufacturer and would have to be experimentally determined, as well as greatly varying thicknesses across each membrane, making the measurements quite inconsistent.

### **Data Collection**

During data collection, the force gauge was pressed onto the PDMS membrane until a stable output force of roughly 0.2N was received. This meant that the incremental depressions from the protocols would have a measureable effect on the system's pressure output. The value of 0.2N was decided upon after several empirical tests and was deemed to fit well enough for data collection. Then, either protocol three or four was selected and manually executed using an editable text field in the LabView software controlling the Z-axis of the XYZ-table. For a comprehensive visualization of the two protocols that were used, see Figures 9 & 10.

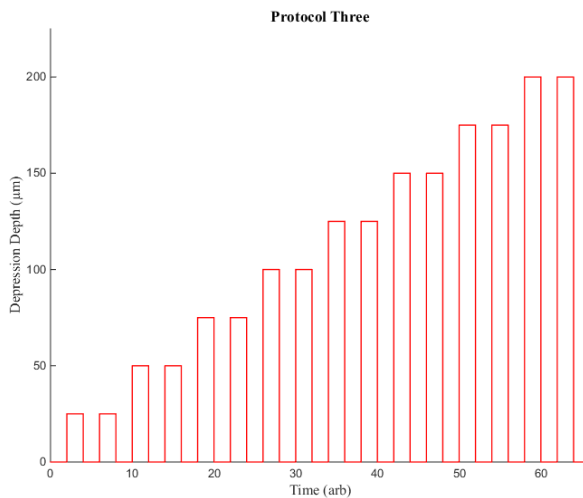


**Figure 9** – The third measurement protocol visualized as units of depression depth vs. arbitrary time. The protocol steps were reflected in the force graph for each measurement, with fluctuations in regards to the timing of each step and the output from the pressure sensors.

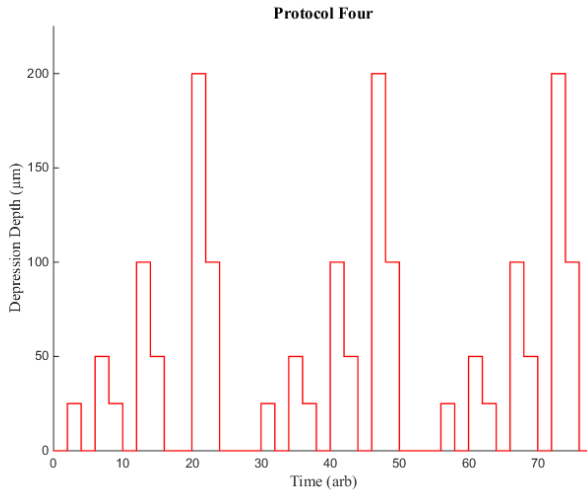


**Figure 10** – The fourth measurement protocol visualized as units of depression depth vs. arbitrary time. The protocol steps were reflected in the force graph for each measurement, with fluctuations in regards to the timing of each step and the output from the pressure sensors.

When extracting data from the measurements of protocol three, one point was selected for each peak as the fifth sampled data entry before the subsequent drop to baseline pressure. Additionally, the change in baseline pressure was estimated for each measurement and if the change was on the scale of 10% of the maximum peak or greater, the data was manually normalized using the baseline pressure previous to each peak. If it was deemed less than 10%, the whole measurement was normalized using the baseline pressure just before the first relevant peak.

Similarly, protocol four measurement data was selected as the fifth sampled raw data entry before the subsequent drop in pressure. However, due to the nature of the protocol, another data point was collected before the pressure dropped to the baseline level.

## Results

The characterization curves for all four membrane thicknesses can be seen in Figure 11, where raw data is indicated with markers and polynomial fits of the second degree (chosen arbitrarily to show data trends) are plotted as solid lines.

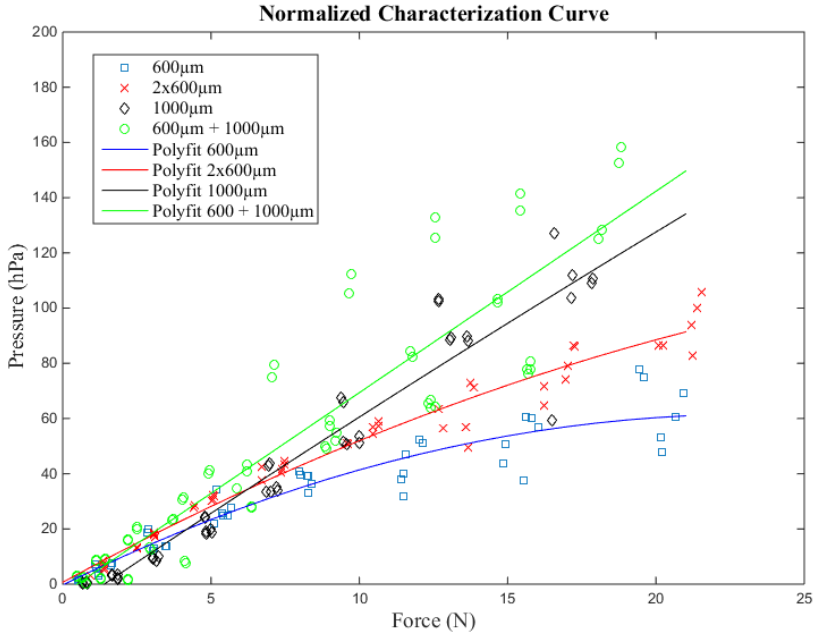


**Figure 11** – Characterization curves for all four membrane thicknesses using the third measurement protocol. The data was normalized according to the baseline pressure for each measurement.

The results from measurement protocol four can be seen in the hysteresis plots 12, 13, 14 and 15.

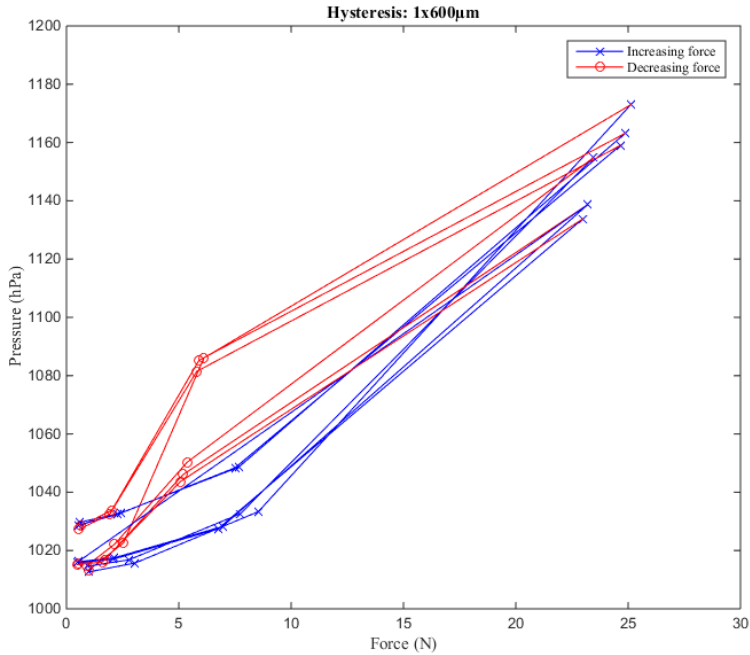


**Figure 12** – Hysteresis data for the 600µm PDMS membrane collected using the fourth measurement protocol. Data points collected from the peaks in the protocol are connected in blue while data collected from plateaus is connected in red. The system’s hysteresis can be gauged by comparison between peaks and plateaus of corresponding depression depth.

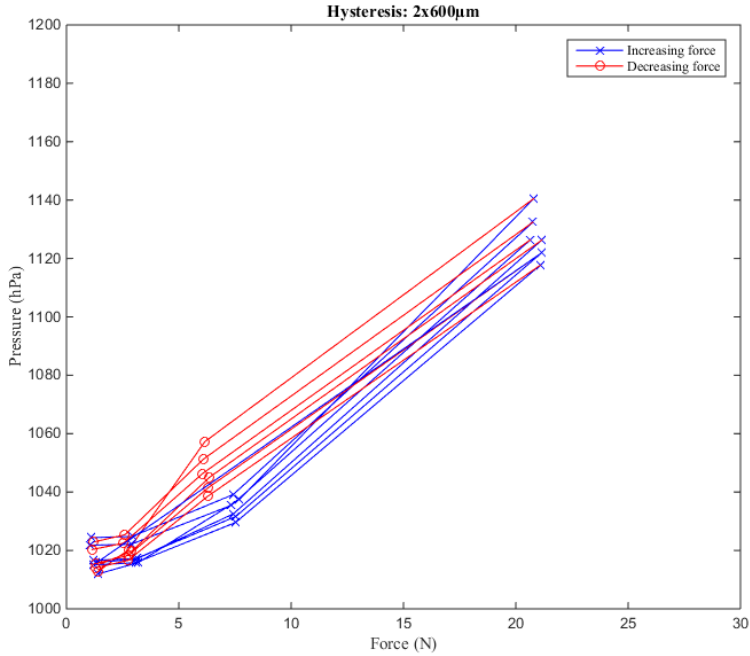


**Figure 13** – Hysteresis data for the 2x600µm PDMS membrane collected using the fourth measurement protocol. Data points collected from the peaks in the protocol are connected in blue while data collected from plateaus is connected in red. The system’s hysteresis can be gauged by comparison between peaks and plateaus of corresponding depression depth.



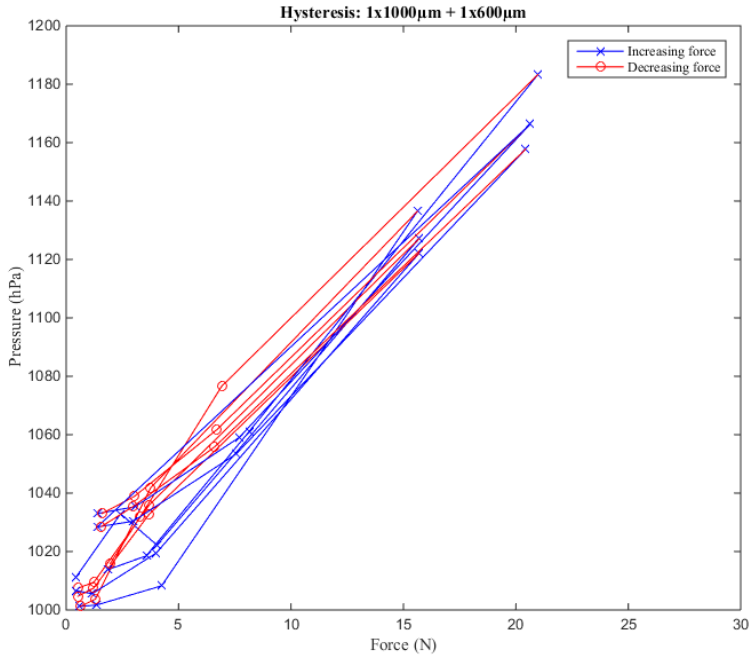


**Figure 14** – Hysteresis data for the 600µm + 1000µm PDMS membrane collected using the fourth measurement protocol. Data points collected from the peaks in the protocol are connected in blue while data collected from plateaus is connected in red. The system’s hysteresis can be gauged by comparison between peaks and plateaus of corresponding depression depth.

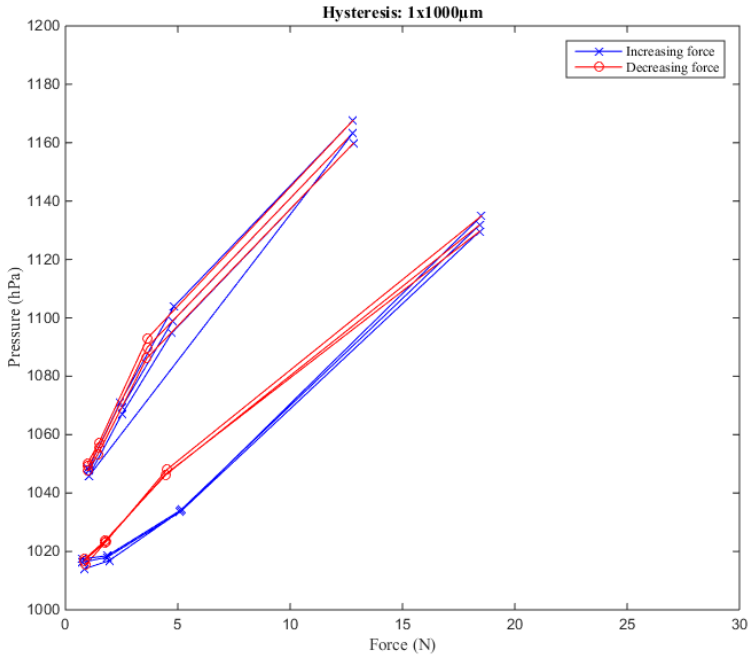


**Figure 15** – Hysteresis data for the 1000µm PDMS membrane collected using the fourth measurement protocol. Data points collected from the peaks in the protocol are connected in blue while data collected from plateaus is connected in red. The system’s hysteresis can be gauged by comparison between peaks and plateaus of corresponding depression depth.

Using the force and pressure response data, the rise time of the system could be calculated by measuring the time between 10% and 90% of the amplitude of a pressure response. Since no direct time data was available from the LabView software, the interval was estimated given a measurement sampling frequency of 5Hz as  $1 < t_{rise} < 8s$ . The speed of the force gauge was found to be on the range of two magnitudes smaller and thus did not limit the rise time.

## Proprioception

### Results

Both types of strain gauges were successfully manufactured and were able to conduct electricity throughout the circuit. However, neither the gold nor copper versions of the produced strain gauges yielded any measurable fluctuations in resistance during bending. However, when contacting the gold polyimide circuits with the copper strips, the resting resistance for each design (denoted with one, two or three dots) could be calculated. These values can be seen in Table 2.

Design	Resistance (k $\Omega$ )
○	1.117
○	$\infty$
○ ○	0.966
○ ○	0
○ ○ ○	1.935
○ ○ ○	0

**Table 2** – Resting resistance values of six lab produced metal-foil strain gauges (two of each sensor design, each design denoted as a collection of dots ranging from one to three).

As the measured data was quite inconsistent and the measurement setup quite flawed, no strain gauge characterization was achieved. The finalized gold strain gauges from two successful attempts in the lab can be seen in Figures 16, 17 and the copper sheet test can be seen in Figure 18.



**Figure 16** – Finished gold foil strain gauges. In order to establish a connection, wiring was attached onto the substrate using silver epoxy glue.

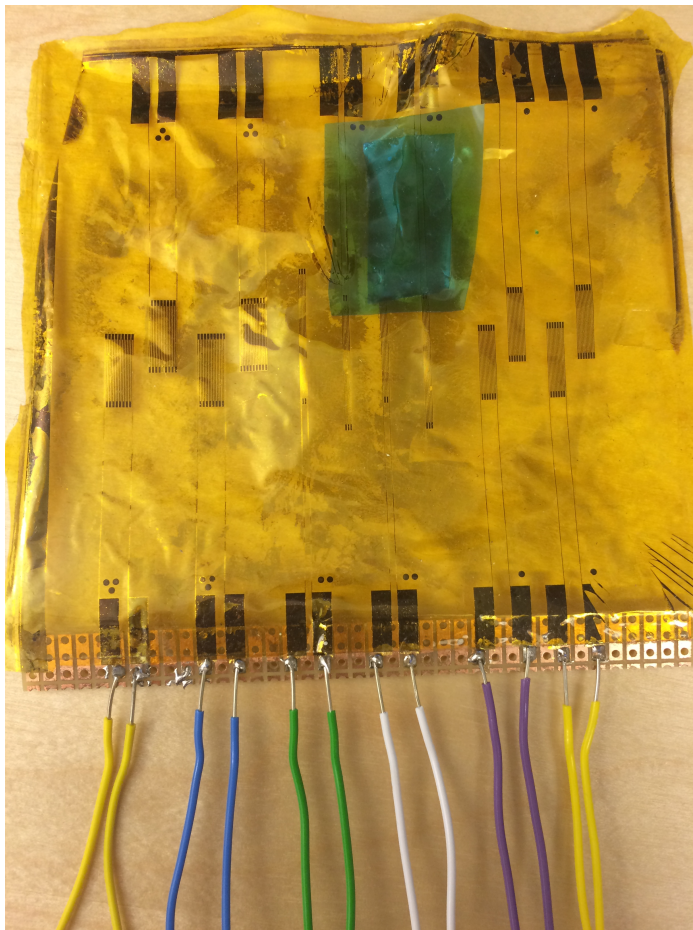


**Figure 17** – Finished gold foil strain gauges. In order to establish a connection, wiring was soldered onto copper strips which were attached to the sample.

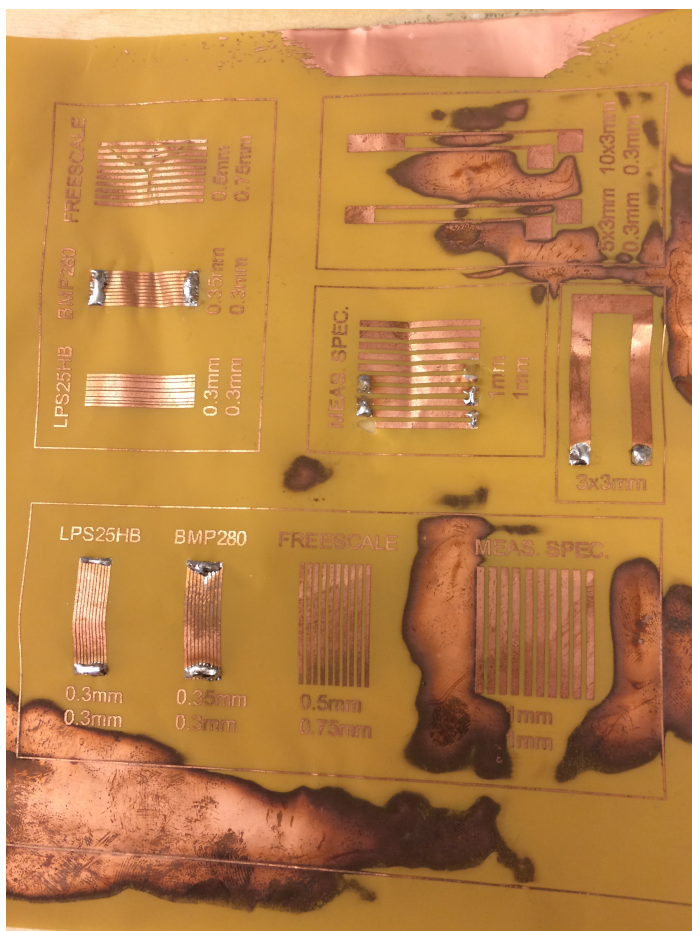


**Figure 18** – Finished copper foil strain gauge test.

Regarding the resolution of the printing method, almost all lines in the pattern were fully etched, save for the supposed 0.3mm spacing between some of the lines.

## Discussion

First, the results, materials and methods of the project are discussed, followed by thoughts on the project as a whole and of future aspects.

The LPS25HB sensors that were sealed in Sylgard170 (or otherwise was in direct contact to its liquid form) displayed many worrying phenomena: heating up quickly and steadily during applied pressure, very slow relaxation speed, extreme temperature dependence and very low response to direct force (on the scale of 1hPa per 50N applied as opposed to nearly 160hPa per 60N applied for the non-sealed sensors). Needless to say, the benefits of having the pressure sensors sealed for stability did not make up for the major loss of functionality that came with it. Subsequently, no data from these was collected toward the end result. The BMP280 sensors that had been sealed displayed a complete lack of functionality. However, in the case of BMP280, the liquid Sylgard170 had fully penetrated the exterior and fully destroyed the sensor.

The characterization curve, seen in Figure 11, relates the applied force to the output pressure and it displays some interesting trends. Firstly, the data sets do not line up according to increasing total membrane thicknesses, but is rather divided into two regimes: the topmost regime of 1000 $\mu$ m and 600 $\mu$ m + 1000 $\mu$ m data and the lower regime of the remaining data sets. Within each regime, however, the data sets line up according to increasing membrane thicknesses. An obvious difference between the two regimes is the fact that the top one contains the thicker, 1000 $\mu$ m PDMS membranes. Thus, individual layer thicknesses within a laminated membrane seems to be an effect on the output of the system.

The large spread of rise time can be attributed to the behaviors of each membrane's system: each membrane creates a sealed system which has a region within which the rise time is stable and

easily measurable. This region shifted depending on the thickness of the membrane and its individual layers, but could often be seen in the range of 1N to 10N. Importantly, this preferred region lies within the most relevant forces for an individual finger of a hand. The other regions, typically at very low or very high forces, tend to differ greatly in shape. For example, some peaks at high forces reach their maximum amplitude at the time of force application and degrade from there. In general, the response time, sensitivity and reproducibility of the system are, however, much better than anticipated and show great promise for future development.

The hysteresis seen in Figures 12 and 13 shows that, with 600 $\mu$ m membranes, the PDMS behaves as you might expect; after the PDMS is initially compressed, it retains part of its compressed state when the force gauge is withdrawn, resulting in a higher pressure output. The behaviors seen in Figures 14 and 12, however, are somewhat different. In Figure 14, there is a large variation between individual measurements, alluding to issues during data collection. This is further emphasized by the outliers that can be seen in the 0-5N interval. As for Figure 15, there are two clear regimes with similarly trending data but different offset values. The lowermost data set was collected before the other set and shows a clear hysteresis pattern. The other set, seen at a much higher offset, was collected after grease is suspected to have partially seeped into the sensor's sensing cavity. Thus, the data can be seen as less representative of the fully operational system's characteristics. However, since it still displayed a clear patterned behavior and the system was able to cope extremely well to protocol three tests, it was not removed from the data set. Please note that even though it responded very well to protocol three with very fast and clear responses, it had problems initiating each test run (presumably due to grease partly clogging the surface) and broke down fully after the data was collected.

The strain gauges that were manufactured in the cleanroom were not dysfunctional per se, but were not possible to electrically



measure using the available materials and methods. It was later revealed that the expected change in resistance would be around a  $m\Omega$  while the multimeter could only measure changes on the scale of hundreds of  $m\Omega$ . Therefore, it is still possible that the design and laboratory execution of the gauges were sufficient and could be properly utilized within future projects, even though no relevant data could be extracted. Additionally, while the copper versions were much more simple to manufacture than those with gold, gold gauges are generally preferred due to the notable malleability of gold.

Unfortunately, the resolution tests performed on the copper strain gauge design were not as precise as we had hoped; the size of the pattern features seem to have been restricted more so by the conversion of the design into a printable file format than by the printer itself (both the scale of the image as well as line thicknesses were tampered with, leaving the design adjusted according to low-resolution pixel configurations rather than the sizes defined in the  $100\mu\text{m}$ -range in AutoCAD). However, we can still note that features distanced around  $300\mu\text{m}$  apart from each other were successfully separated, which hints that the copper etching process is compatible with such dimensions.

In conclusion, the constructed pressure-sensing systems showed great potential —especially for  $600\mu\text{m}$  membranes —, but would benefit from a sealing technique which does not compromise the sensor in the way that the grease did. Strain gauges can with little effort be constructed using the ink jet printing method, but their characteristics are not as preferable as those of the gold strain gauges made in a clean room environment. Both types of sensors produced within this project would make promising cornerstones for further research.

## Looking back and ahead

In 1992, Phillips, Johansson, and Johnson published a study regarding the spatial resolution of the human fingertip, revealing

that both fast-response and slow-response afferents of type one (called FA1, SA1) share a spatial resolution of around 1.5mm. In contrast, the resolution for their type-two counterparts (FA2, SA2) came out to 3-4mm. (10) In order to match this input, the number of pressure sensors on each phalange could be extended and placed in a 2D array connecting into a continuous receptive field. As such, more pressure data, from a much larger area of the skin, could be extracted and thus bringing the emulation closer to the feel of a natural skin. However, seeing as the externally applied pressure would be distributed among the pressure sensors through the artificial skin, this could require a more complex process of data processing in order to relay a cohesive pressure image.

As for continued research within mechanoreception for prosthetic skin, it would be interesting to investigate a way to incorporate the remaining properties of the human mechanoreceptive system; vibrational sensation and skin stretch sensations are examples of such features that are naturally available to humans(11). Additionally, the human fingertips are adept at discerning the general curvature of a stimuli. The receptors responsible for curvature sensing, supposedly SA1, were found to be positioned at the periphery of the fingerpad(12). This would imply that they sense the curvature outside of their immediate receptive fields, something that is not trivial for conventional pressure sensors. If curvature sensing is found to be desired in a prosthetic skin, it would be interesting to investigate whether or not it is possible to emulate the SA1 receptor's abilities, deriving curvature information from the pressure relayed through the coating silicone layer.

The choice of flexible coating material within this project can be questioned and remains somewhat arbitrary; reasonably, other, similar, coatings would lead to somewhat similar output characteristics (variations based on molecular structure, mixing ratio, layer thickness etc.). However, any variations of material properties could be mitigated by careful calibration of the pressure out-

put. Here, a silicone coating was chosen due to its gas permeability, malleability, physical durability, accessibility, chemical stability and safety as well as price range. Thus, the question that remains is whether or not an entirely different material would lead to a better performance (whatever that may entail in future applications). Moreover, the thickness of the layer could be adjusted, balancing between a durability and sensitivity trade-off. It is important to note, however, that the current project was more qualitative than quantitative in nature, desiring to probe the feasibility of the skin instead of its optimal performance.

Based off of the findings published in 1995 by Benoni and Johansson, further modifying the silicone layer into a sensing element in itself could improve the proprioception of the artificial skin; by sensing the skin stretch and relating it to extension or flexion patterns of the hand, kinesthetic information could be deduced.[\(13\)](#) That way, information regarding the flexion or extension of digits from the strain gauges could be backed by such skin stretch data, or even render other proprioceptors unnecessary. On a related note, research from 2006 suggests that ionic polymer metal composites (IPMC) can function as proprioceptors by measuring the change in voltage during flexion or extension[\(14\)](#). The sensors proposed within the publication are dynamic, which means that they do not detect absolute bending angles, but rather the change between two angles. The sensors' response to bending is highly linear, displays low error rates and has the ability to detect bending rates. However, due to the fact that their output is affected by both pressure as well as temperature, they would likely not be well suited as the main proprioceptors of a prosthetic device. With that being said, adding such contraptions as back-up sensors (e.g. on the dorsal side of the hand) onto a rig where there already are sensors able to read absolute bending angles would certainly provide data that could refine and secure the accuracy of the output.

Furthermore, there is a question which arises when attempting to mimic the characteristics of the human fingertip: is it desirable

to mirror the mechanical properties of the fingertip when designing a prosthetic hand, considering that the means of sensing are not the same? An article published in 1995 by Srinivasan and LaMotte displayed a clear, nonlinear relation between applied force and depth of indentation of the human fingertip, meaning that the natural finger is able to *cushion* an object for a certain interval before gripping it. Interestingly, the team also compared the compliance of the human finger with that of constructed rubber samples. None of the rubber samples, spanning many levels of compliance, displayed the nonlinear relationship found with the human fingertip.<sup>(15)</sup> Thus, it could be of relevance to study the impact of this nonlinear relationship between applied force and depth of indentation in order to see whether or not such a material works well with electronic pressure sensors.

As mentioned earlier in the report, one restriction of the development was the fact that it took a modest budget into consideration. This is reflected in the choice of coating material, sensors, micro controllers as well as the connections suggested. In early 2015, similar research by Gerratt *et al.* showed that solutions implementing relatively cheap materials (e.g. silicone foam, PDMS, Au/Cr traces) do, indeed, show great promise<sup>(16)</sup>. Utilizing pressure sensors and resistive strain gauges, this research demonstrates a wearable, elastomer-based electronic skin in the shape of a glove. Much like what was proposed earlier, the skin was able to cover a large area of each finger as opposed to discrete positions. This can be attributed mainly to their pressure-sensing elements, which were composed of a dielectric foam layer with conductive microcracked gold on each side.

Similarly, Wettels *et al.* showed an example of a pressure sensitive element able to sense pressure changes continually over an area the size of a fingertip in 2008. The experiment was driven by the notion that robotics in the industry were severely limited due to their lack of touch feedback refWettels08. This technology was powerful enough to break through to the market on its own, culminating in the company now called SynTouch LLC and

its sensor products. This shows that even the robotics industry could benefit from a lower-cost tactile sensory feedback mechanism such as a prosthetic skin. In such a scenario, however, the skin would obviously need to be reworked in order to suit the needs of robotic arms rather than those of the upper-limb amputee.

Additionally, seeing as the pressure sensors used within this project also can measure their surrounding temperature, it is possible that even heat could be transduced to the user's skin. This could, for example, be achieved using a Peltier cooler as a thermoelectric generator, after adjusting for the effects of the covering silicone layer.

## Concluding Remarks

Using the technology described within this thesis as a building block, functional and relatively cheap pressure-sensitive prosthetic skin can surely be achieved. In addition to such a skin being able to increase the performance of the limb as well as regenerating a sense of touch to the user, a future prospect of sensory feedback artificial skin might very well be fitting it to other limb prosthetics aside from hands. Surely, such advances would lead to more intuitive and biomimetic prostheses overall. In summation, the mechanoreceptors devised within this project have shown potential for high pressure resolution, force stability, high sensitivity as well as low production cost.

Continued research based off of this project might benefit from putting an emphasis on the application of said mechanoreceptors as well as on the manufacture of strain gauges used for proprioception, seeing as those were not realized within this project.

## References

- [1] Ortiz-Catalan, M., Håkansson, B. & Brånemark, R. (2014) An osseointegrated human-machine gateway for long-term sensory feedback and motor control of artificial limbs. *Science Translational Medicine*, 6(257), 257.
- [2] Yang, J., Pitarch, E. P., Abdel-Malek, K., Patrick, A. & Lindkvist, L. (2004) A multi-fingered hand prosthesis. *Mechanism & Machine Theory*, 39(6), 555-581.
- [3] Jones, L. (1997) Dextrous hands: human, prosthetic, and robotic. *Presence: Teleoperators & Virtual Environments*, 6(1), 29-56.
- [4] Patterson, P. E. & Katz, J. A. (1992) Design and evaluation of a sensory feedback system that provides grasping pressure in a myoelectric hand. *Journal of Rehabilitation Research & Development*, 29(1), 1-8.
- [5] Biddiss, E., Beaton, D. & Chau, T. (2007) Consumer design priorities for upper limb prosthetics. *Disability & Rehabilitation: Assistive Technology*, 2(6), 346-357.
- [6] Antfolk, C. (2012) Doctoral thesis: On sensory feedback in hand prostheses. *Lunds Universitet*, ISBN: 978-91-7473-282-5.
- [7] Antfolk, C., D'Alonzo, M., Controzzi, M., Lundborg, G., Rosen, B., Sebelius, F., & Cipriani, C. (2012) Artificial redirection of sensation from prosthetic fingers to the phantom hand map on transradial amputees: vibrotactile versus mechanotactile sensory feedback. *Neural Systems & Rehabilitation Engineering*, 21(1), 112-120.
- [8] Simone, L. K. & Kamper, D. G. (2005) Design considerations for a wearable monitor to measure finger posture. *Journal of NeuroEngineering & Rehabilitation*, 2, 5.

- [9] [http://www.sandia.gov/polymer-properties/E1-Youngs\\_modulus.html](http://www.sandia.gov/polymer-properties/E1-Youngs_modulus.html), 2015-12-08.
- [10] Phillips, J. R., Johansson, R. S. & Johnson, K. O. (1992) Responses of human mechanoreceptive afferents to embossed dot arrays scanned across fingerpad skin. *The Journal of Neuroscience*, 12(3), 827-839.
- [11] Johnson, K. O. (2001) The roles and functions of cutaneous mechanoreceptors. *Current Opinion in Neurobiology*, 11(4), 455-461.
- [12] Bisley, J. W., Goodwin, A. W. & Wheat, H. E. (2000) Slowly adapting type I afferents from the sides and end of the finger respond to stimuli on the center of the fingerpad. *The Journal of Neurophysiology*, 84(1), 57-64.
- [13] Benoni, B. E. & Johansson, N. (1995) Skin strain patterns provide kinaesthetic information to the human central nervous system. *The Journal of Physiology*, 487, 243-251.
- [14] Biddiss, E. & Chau, T. (2006) Electroactive polymeric sensors in hand prostheses: bending response of an ionic polymer metal composite. *Medical Engineering & Physics*, 28(6), 568-578.
- [15] Srinivasan, M. A. & LaMotte, R. H. (1995) Tactual discrimination of softness. *The Journal of Neurophysiology*, 73, 88-101.
- [16] Gerratt, A. P., Michaud, H. O. & Lacour, S. P. (2015) Elastomeric electronic skin for prosthetic tactile sensation. *Advanced Functional Materials*, 25(15), 2287-2295.



## Appendix A: Lab Protocol

### UV-mask

Goal: UV-mask able to finely replicate the desired pattern.

1. the pattern design was entered into the mask writer at 20mm-mode
2. developer AZ351B was used to develop the mask for 1min
3. the mask was cleaned with water and dried with nitrogen
4. the mask was etched using a standard chrome etchant for 1.5min and dried with nitrogen

### Pattern Development

Starting from a glass square covered with a polyimide film coated with a little chrome followed by gold. Goal: neatly patterned strain gauges.

1. 4ml AZ1514 positive photoresist was applied to the gold-coated polyimide
2. sample was spun at 1200rpm for 15 s, then 3600rpm for 45s
3. sample was soft-baked at 86°C for 20min
4. the UV-mask and the sample were combined and flashed with UV in the UV-lithography machine for 11s
5. developer AZ351B was used to develop the sample for 3min
6. sample was etched in a gold etch solution of potassium iodide for 1min
7. sample was cleaned with ethanol and water and dried with nitrogen
8. sample was etched in a chrome etch solution for 1.5min
9. sample was cleaned with water and dried with nitrogen

## Surface Protection

Goal: neatly patterned strain gauges with protection on the active side.

1. the connective ends of the gold design were covered with very weak tape
2. sample was protected with 4ml Durimide7505 spun at 3600rpm for 30s
3. all tape was removed and the sample was soft-baked at 90°C for 15min
4. the UV-step was repeated for 15s and the sample was left to rest at room temperature for 1hr
5. sample was rinsed with the developer HTR-D2 followed by the rinser RER600
6. sample was placed in an oven for 2h, letting it cool overnight

## PDMS Application

Goal: neatly patterned, protected strain gauges with PDMS on the inactive side.

1. standard Sylgard184 PDMS was mixed 10:1 and 20ml was spun onto the sample in two stages: 300rpm for 30s followed by 450rpm for 60s
2. the PDMS was left to reflow for a few minutes before entering the oven at 60°C for 12h

## Appendix B: Arduino Code

Final version of the Arduino code used for data collecting from LPS25HB sensors:

```

/*
Communicates with a LPS25H/HB unit using the SPI interface.
Returns pressure and temperature data to the serial
monitor.

Circuit:
GND/Vcc: USB
CS: D10
SPC: D13
MOSI: D11
MISO: D12

Created by Axel Ekman, 2015-09-02
Last modified 2015-10-13
*/

// libraries
#include <SPI.h>

// constants
// defining 4 pins for SPI (4-wire communication interface)
const int chipSelectPin = 10; // chip select
const int mosiPin = 11; // master out slave in
const int misoPin = 12; // master in slave out
const int clockPin = 13; // SCL clock

// register addresses, written as WRITE default, MS = 0
const byte PRESSURE_LSB = 0x28; // LSB of pressure register
address
const byte PRESSURE_MID = 0x29; // middle byte of pressure
register address
const byte PRESSURE_MSB = 0x2A; // MSB of pressure register
address

const byte TEMPERATURE_LSB = 0x2B; // LSB temperature register
address
const byte TEMPERATURE_MSB = 0x2C; // MSB temperature register
address

const byte WHO_AM_I = 0x0F; // register address for WHO_AM_I
const byte CTRL_REG1 = 0x20; // register address for control
register
const byte RES_CONF = 0x10; // register address for pressure
and temperature resolution configuration

// set variables
const int READ = 0x80; // '10000000' LPS25H read command,
first bit corresponds with R/W; second with MS
const int INCR = 0x40; // '01000000' LPS25H auto increment
command, MS = 1
const int WRITE = 0x00; // '00000000' LPS25H write command

```

```

const int POWERUP = 0x80; // '10000000' LPS25H power-up
      command
const int POWERDOWN = 0x00; // '00000000' Empty byte, resets
      the CTRL_REG1 register (preferences restored in powerUp-
      function)
const int PRESSURE_RESOLUTION = 0x03; // '00000011' provides a
      resolution of 512
const int TEMPERATURE_RESOLUTION = 0x0C; // '00001100'
      provides a resolution of 64
const int BLOCK_DATA_UPDATE_ON = 0x04; // '00000100' turns on
      the block data update function
const int RESET_AZ = 0x02; // '00000010' resets the autozero
      function
const int DATA_OUTPUT_RATE = 0x40; // '01000000' LPS25H
      setting for data output rate of 25 Hz (pressure) / 25 Hz (
      temp)

// settings
int CTRLsettings = POWERUP | BLOCK_DATA_UPDATE_ON |
      DATA_OUTPUT_RATE; // value of desired CTRL_REG1 settings
int RESsettings = PRESSURE_RESOLUTION | TEMPERATURE_RESOLUTION
      ; // value of desired RES_CONF settings

// variables
int counter = 1; // for easy X-axis plotting of data

void setup() {
  // begin
  SPI.begin(); // sets SCK, MOSI & SS as OUTPUTS, pulls SCK
      and MOSI to LOW and SS to HIGH
  Serial.begin(115200);
  // reset the sensor before starting it up
  powerDownLPS25H();
  powerUpLPS25H();

  // SPI setup
  SPI.setBitOrder(MSBFIRST); // the LPS25H sensor operates
      with MSB endianness
  SPI.setDataMode(SPI_MODE3); // clock polarity = 1 (inactive
      high), clock edge = 0 (bit starts at falling slope)
  SPI.setClockDivider(SPI_CLOCK_DIV64); // one 64th of the
      system clock frequency

  // pinModes
  pinMode(misoPin, INPUT);
  pinMode(mosiPin, OUTPUT);

  // leeway time for setup
  delay(5000); // enough time to start data capture
}

void loop() {
  Serial.print(counter);
  Serial.print(",");
  counter++;

  getData();
}

```

```

    delay(200); // so as not to flood the serial monitor
}

// additional functions

void getData(){
    // collects pressure and temperature data and prints it out
    // in the serial monitor
    byte pressure_lsb, pressure_mid, pressure_msb, temp_lsb,
        temp_msb = 0;
    int32_t pressure_tot, temp_tot = 0;
    double pressure_tot_double, temp_tot_double = 0; // cannot
        have (double)pressure_tot = ...

    digitalWrite(chipSelectPin, LOW); // start burst read

    SPI.transfer((READ | INCR) | PRESSURE_LSB);
    pressure_lsb = SPI.transfer(0xFF);
    pressure_mid = SPI.transfer(0xFF);
    pressure_msb = SPI.transfer(0xFF);
    temp_lsb = SPI.transfer(0xFF);
    temp_msb = SPI.transfer(0xFF);

    digitalWrite(chipSelectPin, HIGH); // end burst read

    // shift data, add, convert to hPa
    pressure_tot = (int32_t)((int8_t)pressure_msb) << 24 | (
        int32_t)pressure_mid << 16 | (int32_t)pressure_lsb << 8;
    pressure_tot = pressure_tot >> 8;
    pressure_tot_double = ((double)pressure_tot)/4096.0;

    temp_tot = (int16_t)temp_msb << 8 | (int16_t)temp_lsb;
    temp_tot_double = 42.5 + ((double)temp_tot)/480.0;

    // for testing; contains plain text
    // printValues(pressure_tot_double, temp_tot_double);

    // for data collection; only data
    printData(pressure_tot_double, temp_tot_double);
}

void printData(double pressure, double temperature){
    Serial.print(counter);
    Serial.print(",");
    Serial.print(pressure);
    Serial.print(",");
    Serial.println(temperature); // newline
}

void printValues(double pressure, double temperature){
    Serial.print("Temp:_");
    Serial.print(temperature);
    Serial.println("_C");
    Serial.print("Pres:_");
    Serial.print(pressure);
    Serial.println("_hPa");
}

```

```

    Serial.println(); // newline
}

void powerUpLPS25H(){ // powers up the LPS25H sensor, sets
    data output rate, and temp/pressure resolution
    uint8_t currentStatus = readFromRegister(CTRL_REG1); // ISO
    C++ forbids comparison between pointer and integer, thus
    readFromRegister cannot be used directly in the if-
    statement

    if(currentStatus < 128){ // power up/down is controlled by
        the MSB, meaning it will never contain less than 128 if
        already powered on
        // power up and set CTRL_REG1 settings
        int startCommand = POWERUP | DATA_OUTPUT_RATE; // merge
        powerup-command with data output rate-command
        startCommand = BLOCK_DATA_UPDATE_ON | startCommand; //
        merge with BDU function command
        startCommand = RESET_AZ | startCommand; // merge with
        reset autozero command
        startCommand = startCommand | currentStatus; // merge with
        current information so as not to overwrite (all
        default values are 0)

        writeToRegister(CTRL_REG1, startCommand); // writes the
        power up-command and settings

        // set the temp/pressure resolution
        int resolutions = TEMPERATURE_RESOLUTION |
        PRESSURE_RESOLUTION; // merge the two commands into
        one byte
        writeToRegister(RES_CONF, resolutions); // write the
        resolution to the register

        // update currentStatus and check settings
        currentStatus = readFromRegister(CTRL_REG1);
        uint8_t RESStatus = readFromRegister(RES_CONF);

        checkSettings(currentStatus, RESStatus);
    }

    // if it is already powered up, do nothing
}

void checkSettings(uint8_t CTRL_settings, uint8_t RES_settings
){ // checks if the desired settings have been acquired
    if(CTRL_settings != CTRLsettings && RES_settings !=
        RESsettings){
        Serial.println("##_error_at_both_CTRL_REG1_and_RES_CONF_
            settings_##");
        Serial.println(); // newline
    }

    else if(CTRL_settings != CTRLsettings){ // if CTRL_REG1
        unsuccessful, display its values
        Serial.println("##_error_at_CTRL_REG1_settings_##");
        Serial.println(); // newline
    }
}

```

```

    }

    else if (RES_settings != RESsettings){ // if RES_CONF
        unsuccessful, display its values
        Serial.println("##_error_at_RES_CONF_settings_##");
        Serial.println(); // newline
    }
}

void powerDownLPS25H(){ // powers down the LPS25H sensor and
    REMOVES any previous settings in the CTRL_REG1 register
    uint8_t currentStatus = readFromRegister(CTRL_REG1); // ISO
    C++ forbids comparison between pointer and integer, thus
    readFromRegister cannot be used directly in the if-
    statement

    if(currentStatus >= 128){ // power up/down is controlled by
        the MSB, meaning it will never contain 128 or more if
        already powered down
        writeToRegister(CTRL_REG1, POWERDOWN); // writes the power
        down-command, restoring the byte to 0
    }
    // if it is already powered down
    Serial.println(Device already powered down[U+FFFF]);
}

void whoAmI(byte registerAddress){ // device identification
    uint8_t device_id = (uint8_t) readFromRegister(WHO_AM_I); //
    reads the WHO_AM_I address
    Serial.print("WHO_AM_I: ");
    Serial.println(device_id);
    Serial.println(); // newline
}

uint8_t readFromRegister(byte registerAddress){ // read one
    byte from the specified register. NB. the result is
    UNSIGNED
    digitalWrite(chipSelectPin, LOW); // select sensor

    SPI.transfer(READ | registerAddress); // add the READ
    command (1) to the MSB
    uint8_t result = SPI.transfer(0xFF); // save the returned
    number by sending a full byte

    digitalWrite(chipSelectPin, HIGH); // de-select sensor
    return result;
}

void writeToRegister(byte registerAddress, byte command){ //
    write to the specified register
    digitalWrite(chipSelectPin, LOW); // select sensor

    SPI.transfer(WRITE | registerAddress); // add the WRITE
    command (0) to the MSB
    SPI.transfer(command); // send the command

    digitalWrite(chipSelectPin, HIGH); // de-select sensor

```

}